Phase Imaging Using A Polychromatic X-ray Laboratory Source

B.D. Arhatari, K. Hannah, E. Balaur, A.G. Peele

Department of Physics, LaTrobe University, Victoria 3086, Australia
**Corresponding author: b.arhatari@latrobe.edu.au*

Abstract: We describe a quantitative phase imaging process using an x-ray laboratory-based source with an extremely broad bandwidth spectrum. The thickness of a homogeneous object can be retrieved by using separately spectrally weighted values for the attenuation coefficient and the decrement of the real part of the refractive index. This method is valid for a wide range of object types, including objects with an absorption edge in the used energy range. The accessibility of conventional x-ray laboratory sources makes this method very useful for quantitative phase retrieval of homogeneous objects. We demonstrate the application of this method for quantitative phase retrieval imaging in tomographic measurements.

OCIS codes: (340.0340) X-ray optics; (340.7440) X-ray imaging; (100.5070) Phase retrieval.

References and links

1. A. Snigirev, I. Snigreva, V. Kohn, S. Kuznetsov, and I. Schelokov, "On the possibilities of X-ray phase contrast microimaging by coherent high-energy synchrotron radiation," Rev. Sci. Instrum. **66**, 5486-5492 (1995).
2. D. Gao, T. J. Davis, and S. W. Wilkins, "X-ray phase contrast imaging study of voids and fibres in a polymer matrix," Aust. J. Phys. **48**, 103-111 (1995).
3. R. Toth, J. C. Kieffer, S. Fourmaux, and T. Ozaki, "In-line phase contrast imaging with a laser-based hard x-ray source," Rev. Sci. Instrum. **76**, 0837011-0837016 (2005).
4. F. Zernike, "Phase contrast, a new method for the microscopic observation of transparent objects," Physica **IX**, 686-693 (1942).
5. B. Zakharin and J. Stricker, "Schlieren systems with coherent illumination for quantitative measurements," Appl. Opt. **43**, 4786-4795 (2004).
6. K. A. Nugent, T. E. Gureyev, D. F. Cookson, D. Paganin, and Z. Barnea, "Quantitative phase imaging using hard X rays," Phys. Rev. Lett. **77**, 2961-2964 (1996).
7. D. Paganin, S. Mayo, T. E. Gureyev, P. R. Miller, and S. W. Wilkins, "Simultaneous phase and amplitude extraction from a single defocused image of a homogeneous object," J. Microsc. (Paris) **206**, 33-40 (2002).
8. K. A. Nugent, "Partially coherent diffraction patterns and coherence measurement," J. Opt. Soc. Am. A **8**, 1574-1579 (1991).
9. B. D. Arhatari, A. P. Mancuso, A. G. Peele, and K. A. Nugent, "Phase contrast radiography: Image modelling and optimization," Rev. Sci. Instrum. **75**, 5271-5276 (2004).
10. D. Paganin and K. A. Nugent, "Noninterferometric phase imaging with partially coherent light," Phys. Rev. Lett. **80**, 2586-2589 (1998).
11. S. C. Mayo, P. R. Miller, S. W. Wilkins, T. J. Davis, D. Gao, T. E. Gureyev, D. Paganin, D. J. Parry, A. Pogany, and A. W. Stevenson, "Quantitative X-ray projection microscopy: phase-contrast and multi-spectral imaging," J. Microsc. **207**, 79-96 (2002).
12. J. M. Cowley, *Diffraction Physics*, 3rd revised ed. (North-Holland, Amsterdam, 1995).
13. B. D. Arhatari, F. De Carlo, and A. G. Peele, "Direct quantitative tomographic reconstruction for weakly absorbing homogeneous phase objects," Rev. Sci. Instrum. **78**, 0537011-0537015 (2007).
14. G. R. Myers, S. Mayo, T. E. Gureyev, D. Paganin, and S. W. Wilkins, "Polychromatic cone-beam phase-contrast tomography," Phys.Rev. A **76**, 1-4 (2007).
15. A. G. Peele, F. De Carlo, P. J. McMahon, B. B. Dhal, and K. A. Nugent, "X-ray phase contrast tomography with a bending magnet source," Rev. Sci. Instrum. **76**, 837071-837075 (2005).
16. A. C. Kak and M. Slaney, *Principles of Computerized Tomographic Imaging* (IEEE Press, New York, 1988).
17. B. D. Arhatari, A. G. Peele, K. A. Nugent, and F. De Carlo, "Quality of the reconstruction in x-ray phase contrast tomography," Rev. Sci. Instrum. **77**, 0637091-0637096 (2006).

#102634 - $15.00 USD Received 10 Oct 2008; revised 2 Nov 2008; accepted 12 Nov 2008; published 19 Nov 2008

1. Introduction

Objects with a low electron density, such as low Z and low density materials, can show very little attenuation when imaged with x-rays. However, the interaction cross section for the phase shift of an incident beam can be three orders of magnitude larger than that for absorption. This means that while the absorption contribution can be negligible in an image significant phase contrast can be achieved [1]. Phase contrast as a qualitative imaging tool is thus very useful for imaging materials such as biological samples or polymers. There are many techniques for phase contrast visualization for x-rays: diffraction enhanced imaging [2]; free space propagation phase contrast imaging [1,3]; Zernike phase contrast [4]; and Schlieren phase contrast [5] have all been demonstrated. Each technique has its advantages and its drawbacks with respect to the accessible phase information, the complexity of the setup, the requirements on the beam and the resolution obtainable.

Phase *retrieval* [6, 7], on the other hand, represents a considerable advance over phase contrast images, which typically are seen as edge enhancement or other modulations of the object structure. In phase retrieval it is possible, under common conditions in x-ray imaging, to obtain a quantitative measure of some materials property of a sample. In general this is the projection of δ, which is the decrement from unity of the real part of the complex refractive index: $n=1-\delta-i\beta$, where β is related to the linear attenuation coefficient by: $\mu = 4\pi\beta/\lambda$. In certain cases this phase information can also be obtained for samples that exhibit significant absorption. Another advantage of applying a phase retrieval algorithm to image contrast data is that the resulting image, which gives the projection of δ, looks similar to an absorption contrast map of the sample, which gives the projection of β. This makes interpretation simpler for researchers familiar with absorption contrast.

In phase imaging the coherence of the beam is an important factor in determining the image quality. The effect of spatially imperfect coherence can be approximated by convolving the image obtained with coherent illumination with a function that has a characteristic width directly related to the inverse of the coherence length [8]. The resulting effect is a blurring of the image [9]. The effect of temporally imperfect coherence (polychromaticity) in the beam can also produce blurring in the image [10]. This is often disregarded when a sufficiently small bandwidth, such as through a monochromator, is available. However, in a laboratory-based x-ray source, narrowing the bandwidth greatly reduces the incident flux and leads to a decrease in the signal to noise ratio. Methods that can use a broader bandwidth will therefore make better use of the available flux from a laboratory source. Some methods of choosing an effective wavelength from the spectrum distribution have previously been introduced for phase imaging [10,11] but these approaches are valid only for a narrow bandwidth where the refractive index varies linearly as a function of energy or when using a quasi linear energy spectrum distribution [10]. This article describes a free space propagation based phase retrieval imaging process using an x-ray laboratory source with a very broad bandwidth so that signal to noise can be maximized.

2. Polychromatic phase retrieval

In a monochromatic beam, the transport of intensity (TIE) equation can be used to describe the propagation of the transmitted wave function as [6]:

$$\frac{\partial I_\lambda^z(\boldsymbol{r})}{\partial z} = -\frac{\lambda}{2\pi}\nabla\cdot\left[I_\lambda^0(\boldsymbol{r})\nabla\varphi_\lambda(\boldsymbol{r})\right], \tag{1}$$

where $I_\lambda^{z,0}$ is the intensity at wavelength, λ, measured at a propagation distance, z, 0, φ_λ is the phase of the wave leaving the sample and ∇ is the gradient operator. Assuming an almost homogeneous absorption $(\partial\mu/\partial r \approx 0)$, it can be shown that [12]:

$$I_\lambda^z(\boldsymbol{r}) = I_\lambda^0(\boldsymbol{r})\left[1-\frac{z\lambda}{2\pi}\nabla^2\varphi_\lambda(\boldsymbol{r})\right]. \tag{2}$$

#102634 - $15.00 USD Received 10 Oct 2008; revised 2 Nov 2008; accepted 12 Nov 2008; published 19 Nov 2008

For a homogeneous object (one that is composed of a single material), the variation of the phase and intensity in the object plane can be expressed in terms of the projected thickness of the sample, ***T(r)***, in the plane perpendicular to the projection direction [7]:

$$I_\lambda^0(\boldsymbol{r}) = I_\lambda^{in}(\boldsymbol{r}) e^{-\mu_\lambda T(\boldsymbol{r})}, \qquad \varphi_\lambda(\boldsymbol{r}) = -\frac{2\pi}{\lambda}\delta_\lambda T(\boldsymbol{r}), \tag{3}$$

where I_λ^{in} is the intensity entering the sample, and μ_λ and δ_λ are the monochromatic values for μ and δ. It follows that Eq. (2) can be written as:

$$I_\lambda^z(\boldsymbol{r}) = I_\lambda^{in}(\boldsymbol{r}) e^{-\mu_\lambda T(\boldsymbol{r})}\left[1 + z\delta_\lambda \nabla^2 T(\boldsymbol{r})\right]. \tag{4}$$

The first order expansion of Eq.(4), obtained in the weakly absorbing sample limit, gives [13]:

$$I_\lambda^z(\boldsymbol{r}) = I_\lambda^{in}(\boldsymbol{r})\left[1 - \mu_\lambda T(\boldsymbol{r}) + z\delta_\lambda \nabla^2 T(\boldsymbol{r})\right]. \tag{5}$$

For a broad band source, the quantity that is measured is the integrated intensity across all wavelengths as modified by the detector response function and the interaction with the optical path in the measurement system that lies outside the sample – this last item might include the absorption in the air path or a sample substrate. Accordingly, the measured intensity from a polychromatic source can be written in the weak homogeneous object limit as:

$$I_{poly}^z(\boldsymbol{r}) = \int I_\lambda^{in}(\boldsymbol{r}) D(\lambda)\left[1 - \mu_\lambda T(\boldsymbol{r}) + z\delta_\lambda \nabla^2 T(\boldsymbol{r})\right] \mathrm{d}\lambda, \tag{6}$$

where $D(\lambda)$ is the combined detector response and optical path function. Incident intensity is:

$$I_{poly}^{in}(\boldsymbol{r}) = \int I_\lambda^{in}(\boldsymbol{r}) D(\lambda)\,\mathrm{d}(\lambda). \tag{7}$$

We can define an effective absorption coefficient:

$$\mu_{poly} = \frac{\int \mu_\lambda I_\lambda^{in}(\boldsymbol{r}) D(\lambda)\,\mathrm{d}\lambda}{\int I_\lambda^{in}(\boldsymbol{r}) D(\lambda)\,\mathrm{d}\lambda}, \tag{8}$$

with δ_{poly} defined similarly. Accordingly, we can replace the wavelength dependant terms on the right hand side of Eq.(6) as follows:

$$I_{poly}^z(\boldsymbol{r}) = I_{poly}^{in}\left[1 - \mu_{poly} T(\boldsymbol{r}) + z\delta_{poly} \nabla^2 T(\boldsymbol{r})\right] \tag{9}$$

In the Fourier domain, the Laplacian has a simple expression given by $\mathbb{F}\left[\nabla^2 T(\boldsymbol{r})\right] = -\boldsymbol{u}^2 \mathbb{F}\left[T(\boldsymbol{r})\right]$, where $\mathbb{F}$ is the Fourier transform operator and $\boldsymbol{u}$ is the Fourier variable conjugate to $\boldsymbol{r}$. The two dimensional Fourier transform of both sides of Eq.(9) gives:

$$\mathbb{F}\left[\frac{I_{poly}^z(\boldsymbol{r})}{I_{poly}^{in}(\boldsymbol{r})} - 1\right] = \left(-\mu_{poly} - z\delta_{poly}\boldsymbol{u}^2\right)\mathbb{F}\left[T(\boldsymbol{r})\right], \tag{10}$$

which can then be solved for the thickness as:

$$T(\boldsymbol{r}) = -\mathbb{F}^{-1}\left(\frac{1}{\mu_{poly} + z\delta_{poly}\boldsymbol{u}^2}\mathbb{F}\left[\frac{I_{poly}^z(\boldsymbol{r})}{I_{poly}^{in}(\boldsymbol{r})} - 1\right]\right) \tag{11}$$

This expression can easily be evaluated as we can measure $I_{poly}^z(\boldsymbol{r})$ and $I_{poly}^{in}(\boldsymbol{r})$ directly from experiments, while μ_{poly} and δ_{poly} can be calculated using the measured spectral distribution of the beam and knowledge of the detector response and experimental setup. Simulations under the conditions described above show excellent agreement for the recovered thickness of an object. Accordingly, we now turn to a demonstration of our experimental results using this approach.

3. **Experimental results**

3.1. Sample with no absorption edge

The sample in this experiment is a step sample made from a polyimide film (Kapton, $C_{22}H_{10}N_2O_4$) with a density of 1.45g/cm^3. Each step is a 13 μm thick Kapton layer and the sample is formed with a total of 4 layers. The thickest part is 52 μm. The experiment was

#102634 - $15.00 USD Received 10 Oct 2008; revised 2 Nov 2008; accepted 12 Nov 2008; published 19 Nov 2008

performed with a laboratory-based polychromatic x-ray source (Xradia Inc. micro-XCT). The source has a closed x-ray tube containing Tungsten as a target material and a tube voltage of 40kV was used. The spectrum of the source was measured using an energy sensitive detector (XR-100T-CdTe, AMPTEK Inc.). The detection efficiency of CdTe is approximately 100% in the measured energy range, and the detected histogram is, neglecting absorption in the short air path used and the thin beryllium entrance window to the detector, therefore a good approximation to the source spectrum. The histogram contains a wide continuous energy spectrum (Bremsstrahlung) with some narrow peaks corresponding to the characteristic x-ray energies of the Tungsten target and a cut off energy of 40 keV. The measured spectrum has a low energy cutoff as a result of the detector settings. Additional peaks can also be seen as a result of fluorescence in the detector, but these effects are negligible in our analysis.

The sample is placed at a distance of 60 mm from the approximately 8 μm diameter source and 60 mm from the front part of the imaging detector. The imaging detector is different from the energy sensitive detector mentioned above. The imaging detector is comprised of a scintillator coupled to a CCD camera by a 4x objective lens. With the geometry of the experiment this gives a total image magnification of 8x, and an effective pixel size of 3.3 μm. This point projection is readily converted to the parallel beam case assumed in Eq.(11) using the magnification and an effective propagation distance [7]. The scintillator is made from CsI(Tl) crystal, 300μm thick, wich has high x-ray absorption over the measured energy range and has an edge at 33 keV. Using this knowledge, and relying on a constant coupling of the visible wavelength photons produced by the scintillator to the CCD, the combined detector/experiment response function and the spectrum of the beam can be calculated, with the results shown in Fig. 1(left).

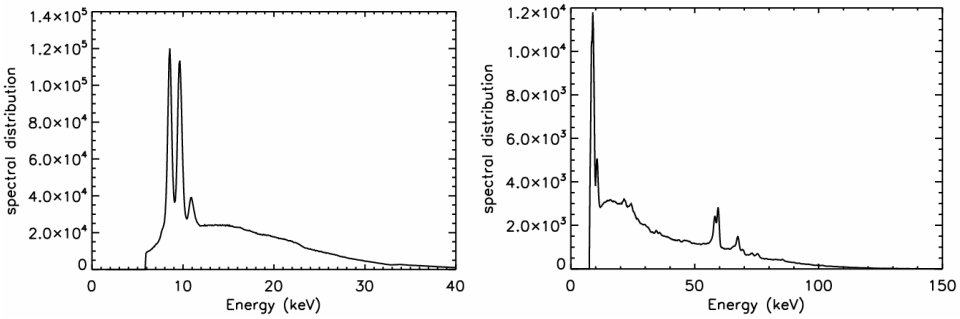

Fig. 1. Combined detector response function and spectrum of the beam for a Tungsten target at 40kV(left) and 150kV(right) tube voltage respectively. The detector artefacts – low energy cutoff and fluorescence peaks – can be seen to have a small effect on the overall spectrum.

The recorded intensity plot of the Kapton step sample obtained by vertically integrating 100 pixels wide of the measured image is shown in the left hand side of Fig. 2. The intensity image was adjusted for the dark current present and for the non-uniform illumination in the imaging system, measured from a reference image of the beam without sample. The edge enhancement typical of phase contrast imaging is clearly visible. The transmission through the thickest part of the sample is approximately 98% thus making the sample a good approximation to the weakly absorbing limit. The retrieved thickness plot is shown in the right hand side of Fig. 2. The solid line represents the retrieved thickness using Eq. (11). The absorption and phase coefficients, μ_{poly} and δ_{poly}, were calculated using the spectral weighting distribution shown in Fig. 1(left). In this case, μ_{poly} is 355.2 m^{-1}, which is equal to the linear attenuation at 10.5keV ($\mu_{10.5keV}$) and δ_{poly} is 2.36×10^{-6} ($\delta_{11.5keV}$). We found that the agreement with the actual thickness is excellent. We also compared the result obtained by choosing a single effective energy and using the corresponding values for μ and δ. An effective energy of 15.5 keV was calculated by making a weighted sum of the energy spectrum of Fig. 1(left). The retrieved thickness using the effective energy is presented as a dashed line. Another

#102634 - $15.00 USD Received 10 Oct 2008; revised 2 Nov 2008; accepted 12 Nov 2008; published 19 Nov 2008

comparison is also made by using the energy at which the spectral weighting distribution peaks (8.3 keV). The retrieved thickness using this energy is presented as a dash-dot line. From the graph it is obvious that both the peak and the effective energy approach are not good methods for retrieving the sample thickness. This is to be expected as μ and δ have different energy dependency of E^{-3} and E^{-2} respectively so a broad band as used here will violate the linear approximation assumed for μ and δ in narrow band approaches [14]. As the approximation to a pure phase object gets better and for narrower bands we therefore also expect to see that the effective wavelength approach will also give reasonable results [15]. The algorithm will assign a generally incorrect value for the thickness in the region covered by the impurity as the assumption about material parameters will be incorrect. The scale of the error will depend on how good the assumption about homogeneity is. In general we find that the reconstruction algorithm is quite stable to the presence of unknown materials, or simply dust, provided such impurities produce no zero intensity in the measured field.

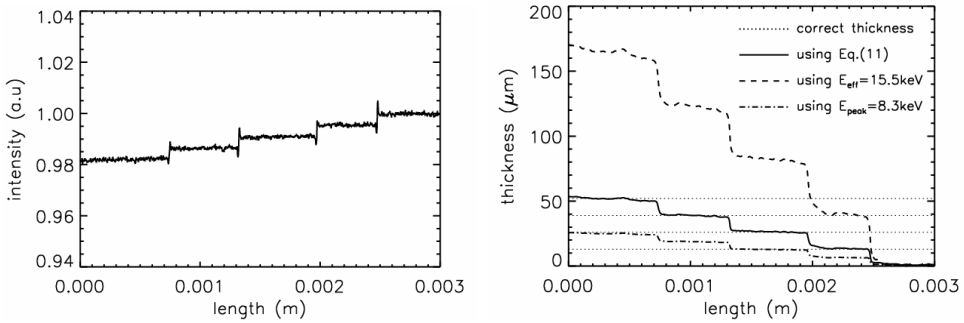

Fig. 2. The recorded intensity plot measured for a polychromatic x-ray source at 40keV (left) and the retrieved thickness plot (right) for the Kapton step sample. The horizontal dotted lines show the actual thickness, the solid line is the retrieved thickness obtained using Eq. (11), the dashed line is the retrieved thickness obtained by using an effective energy, and the dash-dot line is the retrieved thickness obtained by using an energy corresponding to the peak in the spectral weighting distribution shown in Fig. 1.

3.2. Sample with absorption edge

In the second experiment we used a gold sample that has absorption edges (at 12, 14 and 80 keV) in the measured energy range. In this case we used a tube voltage of 150 kV which means the spectrum has a cut-off energy at 150 keV. We took into account the detection efficiency of CdTe and the scintillator absorption in the spectrum distribution (Fig. 1(right)) for this energy range to calculate the corresponding spectral weighting distribution.

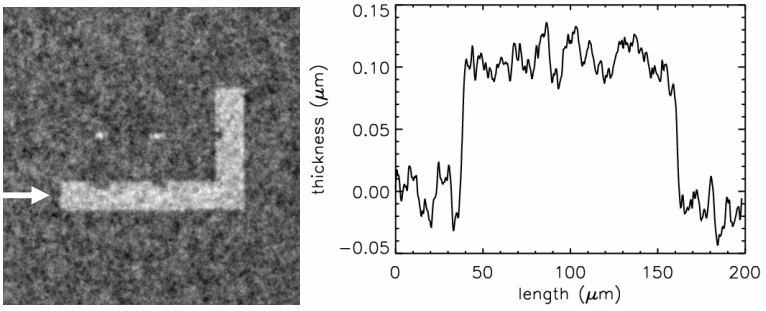

Fig. 3. The retrieved thickness of a 100 nm thick gold sample (left) and a plot (right) of the retrieved thickness along the horizontal line indicated by the arrow.

The gold sample used in the experiment had a thickness of 100 nm, which fulfills the criteria of a weakly absorbing sample. The gold layer in the sample was in the form of the letter 'L' deposited on a thin Silicon Nitrate window. The experimental geometry was the same as for the first experiment with a source-sample distance of 60 mm and sample-detector distance of

#102634 - $15.00 USD Received 10 Oct 2008; revised 2 Nov 2008; accepted 12 Nov 2008; published 19 Nov 2008

60 mm. An objective lens of 20x was used with a 20 μm thick CsI(Tl) crystal as a scintillator. This gave a total image magnification of 40x with an effective pixel size of 0.33 μm. The signal to noise in the detected image is relatively poor due to the low efficiency of the thin CsI scintillator used with the high magnification objective to obtain the high spatial resolution required in this case. The spectral distribution for the 150 kV tube voltage (Fig. 1(right)) was used to calculate μ_{poly} = 99886 m^{-1} ($\mu_{23.2keV}$) and δ_{poly} = 9.39x10^{-6} ($\delta_{18.3keV}$). Using Eq.(11) the retrieved thickness was obtained and is shown in Fig. 3. The thickness of the gold layer was also measured with an Atomic Force Microscope, giving a value of 100 ± 10 nm. This is in excellent agreement with the result shown in Fig. 3. It should be noted that this result cannot be achieved by assuming a pure phase object (μ = 0 m^{-1}) so that while the object is weakly absorbing the incorporation of μ in Eq.(11) is important.

4. Extension to tomography

This method of polychromatic phase retrieval can easily be applied to phase retrieval tomography to reconstruct the δ distribution of the object. By using the well known filtered back projection (FBP) operator [16] applied for phase projection imaging [17], the reconstruction for the polychromatic case can be obtained, as:

$$\delta(\boldsymbol{r}) = FBP\left[\delta_{poly} T^{\theta}(\boldsymbol{r})\right] \tag{12}$$

where $T^{\theta}(\boldsymbol{r})$ is the retrieved thickness for a projection angle, θ. For the phase retrieved tomography experiment we used 42 ± 6.7 μm diameter polystyrene spheres as a sample. A tomography data set was acquired with a tube voltage of 40 kV. In this energy bandwidth, polystyrene (C_9H_{12}, density of 1.05 g/cm^3) has μ_{poly} = 190 m^{-1} ($\mu_{10.1keV}$) and δ_{poly} = 1.88x10^{-6} ($\delta_{11.3keV}$). We used Eq.(11) to retrieve the projected thickness for each projection angle to obtain $T^{\theta}(\boldsymbol{r})$. A total of 721 projections were acquired over an angular range of 180°. A slice reconstructed using Eq.(12) can be seen in the left hand side of Fig. 4. The middle image of Fig. 4 shows a plot of δ_{poly} along a line in the slice as indicated by the arrow. The values obtained for the reconstructed spheres are in excellent agreement with the actual value for δ_{poly}. The area around the center of the spheres shows the correct value. The rounding of regions towards the edges can be attributed to a combination of detector pixel size, system resolution due to finite source size, artefact from the tomography reconstruction and the loss of high spatial frequency information inherent to the phase retrieval process. Our simulations suggest that it is the last of these factors that is, in this case, dominant. In previous work we have shown that it is possible to ameliorate losses in phase contrast by appropriate choice of experiment geometry [9]. The effective voxel size in the reconstruction is (0.41 μm)^3 and the total reconstruction volume contains 490^3 voxels; a volume rendering is shown on the right side of Fig. 4.

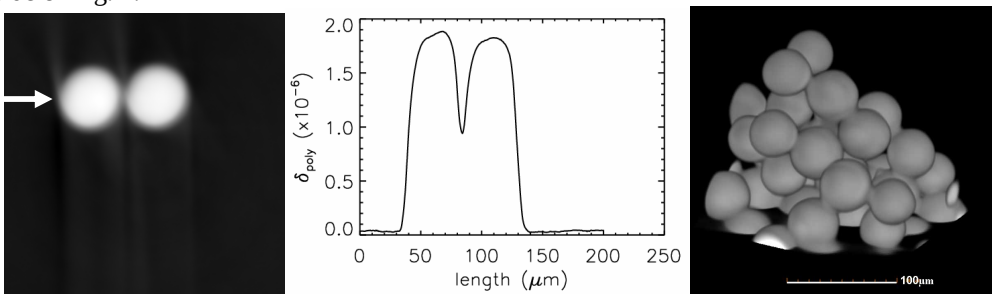

Fig. 4. A reconstructed slice for 42 μm polystyrene spheres (left) imaged using the full spectrum of a laboratory x-ray tube source. The plot (mid) along a horizontal line indicated by the arrow shows the obtained values for δ_{poly}. The image on the right shows a surface rendering for the reconstructed data volume demonstrating that good segmentation for the spheres can be obtained.

#102634 - $15.00 USD Received 10 Oct 2008; revised 2 Nov 2008; accepted 12 Nov 2008; published 19 Nov 2008

5. Conclusion

We conclude that our method is suitable for extremely broad source spectra for phase imaging and that, in the weak object approximation, excellent quantitative reconstructions can be obtained.

Acknowledgments

The authors acknowledge the support of the Australian Research Council through the Centre of Excellence for Coherent X-ray Science and by an APDI fellowship (BDA).

#102634 - $15.00 USD Received 10 Oct 2008; revised 2 Nov 2008; accepted 12 Nov 2008; published 19 Nov 2008